Surface Albedo–Climate Feedback Simulated Using Two-Way Coupling*

BRENT M. LOFGREN

Great Lakes Environmental Research Laboratory, Ann Arbor, Michigan

(Manuscript received 17 August 1994, in final form 25 April 1995)

ABSTRACT

To simulate the effects of feedback between climate and surface albedo via vegetation, a scheme was developed, based on a generalized life zone scheme, for estimating the land surface albedo as a function of annual mean precipitation and surface temperature. This scheme was applied to the climate of a GCM and made interactive with the GCM. The climate of this run was compared with one in which the land surface albedo was prescribed to a spatially uniform value.

Allowing such feedback within the modeling system enhances the atmospheric ascent and heavy precipitation of tropical rainbelts, in comparison with a case with spatially homogeneous surface albedo prescribed. It also intensifies the atmospheric descent and low precipitation rates over subtropical latitudes. That is, a positive feedback occurs at low latitudes. At midlatitudes, thermal forcing due to the spatial distribution of surface albedo has little effect on vertical motion or precipitation. However, in the Central Asian and Gobi Deserts, the high surface albedo cools the surface, reduces evaporative demand, and allows the soil and vegetation to retain more moisture, indicating negative feedback. Because the northern edge of the Sahara has negative feedback similar to that in midlatitudes, while the southern part has positive feedback, the Sahara as a whole is shifted southward when surface albedo feedback is included.

1. Introduction

In Lofgren (1995), experiments were described showing that precipitation and soil moisture are sensitive to prescribed perturbations in surface albedo. Because climate determines the vegetation cover, which influences the surface albedo, these results suggest that the natural state of vegetation can be in some measure self-sustaining by its effects on climate (positive feedback). In this case, human-induced alterations of the vegetation may change the climate in a way that would make it more difficult to restore the vegetation to its previous state. Negative feedback may occur under other conditions, so that the natural vegetation would be self-moderating (tending away from extreme states), and human-induced changes in vegetation might be less persistent. Other studies (e.g., Charney 1975) have suggested that this type of positive feedback occurs in places like the Sahel, but to the author's knowledge, no studies have been published that incorporated explicit feedback into their models by predicting the vegetation cover as a function of climatic variables and using the resulting land surface albedos as input for a general circulation model (GCM). The present study attempts to do this.

Henderson-Sellers and Pitman (1992) discuss the problem of how to predict the vegetation and corresponding land surface parameters, including albedo, based on the climate of a model. As a proposed solution that combines accuracy and simplicity, they suggest the scheme of Henderson-Sellers (1990) for estimating (predicting) the climax vegetation cover based on climate. This method is adapted and used in the present study to simulate feedback among vegetation, land surface albedo, and the natural climate. The Henderson-Sellers scheme is simpler than the schemes of Holdridge (1947), on which it is based, and of Köppen (1936), but includes the influence of temperature on plant growth, which is ignored in Budyko's (1975) radiative index of dryness.

This paper is organized as follows. Section 2 describes the model used here, including the basic atmospheric framework and the method for predicting vegetation and surface albedo. Section 3 describes the experimental strategy and model cases run in this investigation. Section 4 presents the model results. Conclusions from these results are summarized in section 5. Surface albedo feedback into climate is only one aspect of vegetation–climate feedback. The results of Lofgren (1993), which also explored feedback via surface roughness and soil water holding capacity, are briefly summarized in section 5.

* Great Lakes Environmental Research Laboratory Contribution Number 922.

Corresponding author address: Dr. Brent M. Lofgren, NOAA/ERL, 2205 Commonwealth Blvd., Ann Arbor, MI 48105-1593.
E-mail: lofgren@glerl.noaa.gov

2. Model formulation

a. General circulation model

The model used for the simulations discussed in this paper is a version of the Geophysical Fluid Dynamics Laboratory general circulation model, which uses the spectral transform method to solve the equations of motion, thermodynamical equation, and continuity equations of mass and moisture to compute the vertical component of vorticity, horizontal divergence, temperature, surface pressure, and water vapor mixing ratio. The version used here has vertical resolution of nine unevenly spaced sigma layers, and uses rhomboidal-30 horizontal resolution (which transforms to a grid of 3.75° longitude by 2.25° latitude). The main features of the dynamical component of this model are described in Gordon and Stern (1982).

Formulation of radiation, precipitation, moist convection, surface energy, and water balances and adjustment of surface albedo for snow are identical to the description given in Lofgren (1995). Sea surface temperatures are prescribed to observed climatological values. These runs at rhomboidal-30 resolution also include a parameterization for wind drag by internal gravity waves forced by sub-grid-scale topographic features of the surface (Broccoli and Manabe 1992).

b. Prediction of vegetation and surface albedo

The scheme of Henderson-Sellers (1990) "predicts" vegetation in the sense that it tells what type of climax vegetation can be expected to grow, assuming that the climate remains the same for a sufficiently long time. This scheme is extended here by predicting surface albedo based on vegetation. In actual practice, the step is bypassed in which vegetation is predicted, and surface albedo is taken directly from climate. It would perhaps be preferable to develop a scheme that does not implicitly incorporate this two-step process, but that is beyond the scope of this study.

Graphical depictions of the original Holdridge (1947) life zone classification scheme and the modification by Henderson-Sellers are shown in Fig. 1, with life zones as a function of annual mean precipitation and biotemperature. The biotemperature is defined by first calculating monthly mean surface air temperatures (in degrees Celsius), setting to 0 any monthly mean that is lower than 0, and calculating the annual mean after these modifications. The diagonal lines going from the upper left to lower right on each part of Fig. 1 are lines of constant ratio of precipitation to potential evaporation, using Holdridge's approximation that potential evaporation is directly proportional to biotemperature.

Henderson-Sellers (1990) composited Holdridge's (1947) 37 life zones into nine general classifications, as shown in Fig. 1b. Her scheme of climate classification, when applied to observed precipitation data of Legates and Willmott (1990) and surface air temperature data of Oort (1983), does a reasonable job of reproducing the natural vegetation distribution of Küchler (1991), with Africa used as an example in Fig. 2. Approximate equivalencies between the Henderson-Sellers classifications and those of Küchler (1982) have been subjectively determined and are given in Table 1. The most notable difference between Figs. 2a and 2b is that the Henderson-Sellers scheme does not predict the full extent of the rainforests of the Congo Basin, indicating that the precipitation threshold required for classification as a tropical rainforest may be too high. However, better agreement occurs for the extensive rainforests of South America (not shown). Henderson-Sellers (1990), in her Fig. 4, made a similar comparison over Australia.

To assign surface albedo as a function of climate, corresponding classes were selected between the Henderson-Sellers (1990) generalized life zones and the Simple Biosphere Model (SiB) classification scheme (Sellers et al. 1986), which are based on the same classifications as Küchler (1982). A summary of the assumed correspondences, along with the surface albedo for each generalized life zone, is given in Table 2. For the sake of simplicity, surface albedo was not allowed to vary annually, except for the effects of snow, and values were used that are typical of each type of vegetation during the summer season, the time of greatest insolation. These values were taken from Dorman and Sellers (1989), who derived the surface albedo from SiB.

A subjective analysis of surface albedo versus annual precipitation and biotemperature was carried out as shown in Fig. 3, where the Henderson-Sellers classification scheme has been transferred onto a rectangular log–log grid. A notable feature of Fig. 3 is that the change in surface albedo resulting from a given change in precipitation is largest at low values of precipitation, especially since the vertical axis is proportional to the logarithm of precipitation, so that there is a smaller difference in annual precipitation between the horizontal lines near the top than near the bottom.

3. Experiments and analysis strategy

The experimental strategy begins by simulating the climate with a prescribed surface albedo. Next, it is determined what the surface albedo would be, given the "climax" vegetation for that climate, that is, the vegetation that would grow if this climate were to persist until the vegetation came into equilibrium. Next, the climate is simulated again, using the surface albedo of the climax vegetation, and it is determined whether any resulting change in climate changes the surface albedo further from the initial prescribed value (a positive feedback) or changes it back closer to the prescribed value (a negative feedback).

Figure 4 schematically shows the experimental strategy and interpretation of results. A control case was

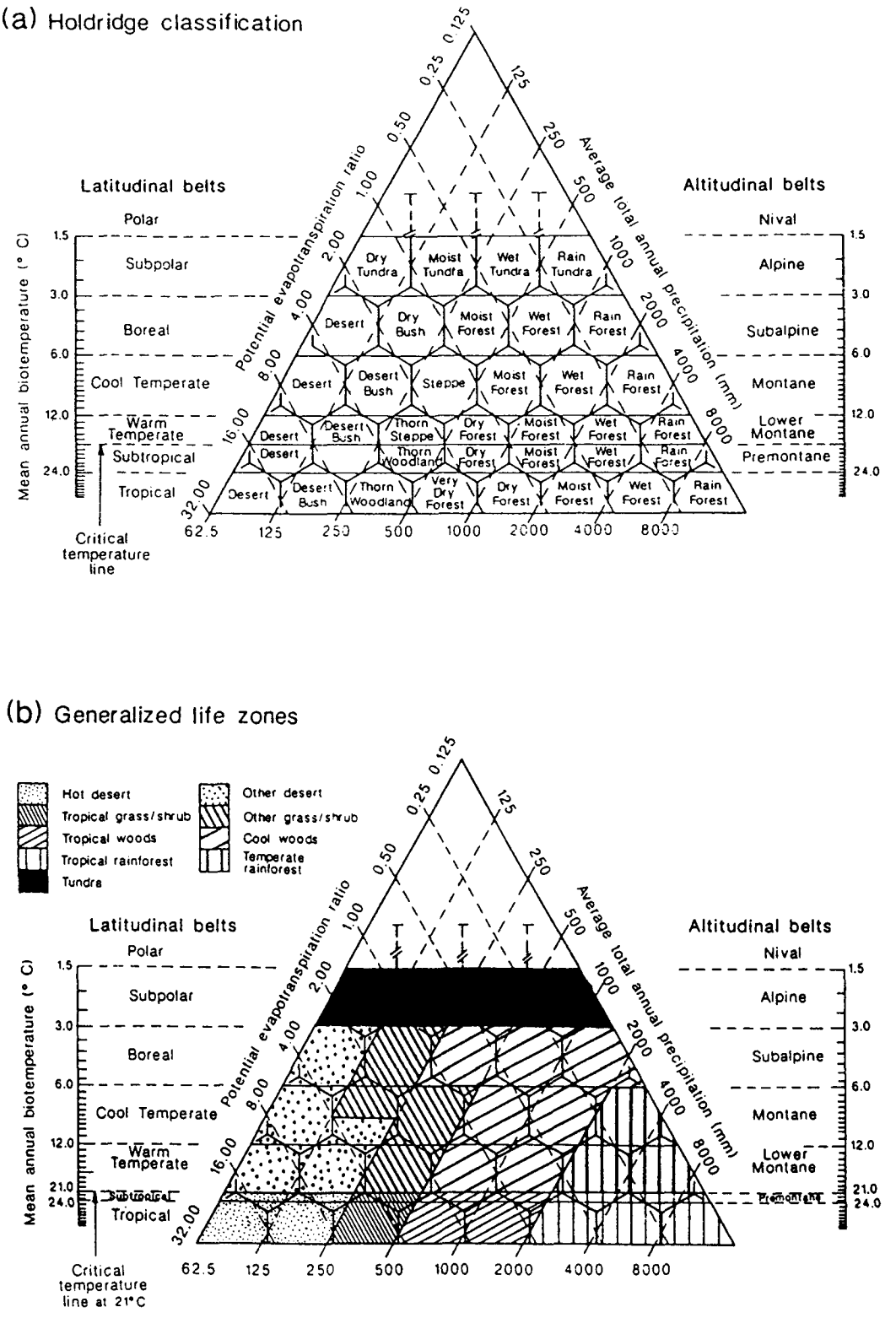

FIG. 1. (a) Life zone classifications of Holdridge (1947) in terms of annual mean precipitation and biotemperature. (b) Generalized life zone classifications proposed by Henderson-Sellers (1990). [Reproduced with permission from Henderson-Sellers (1990).]

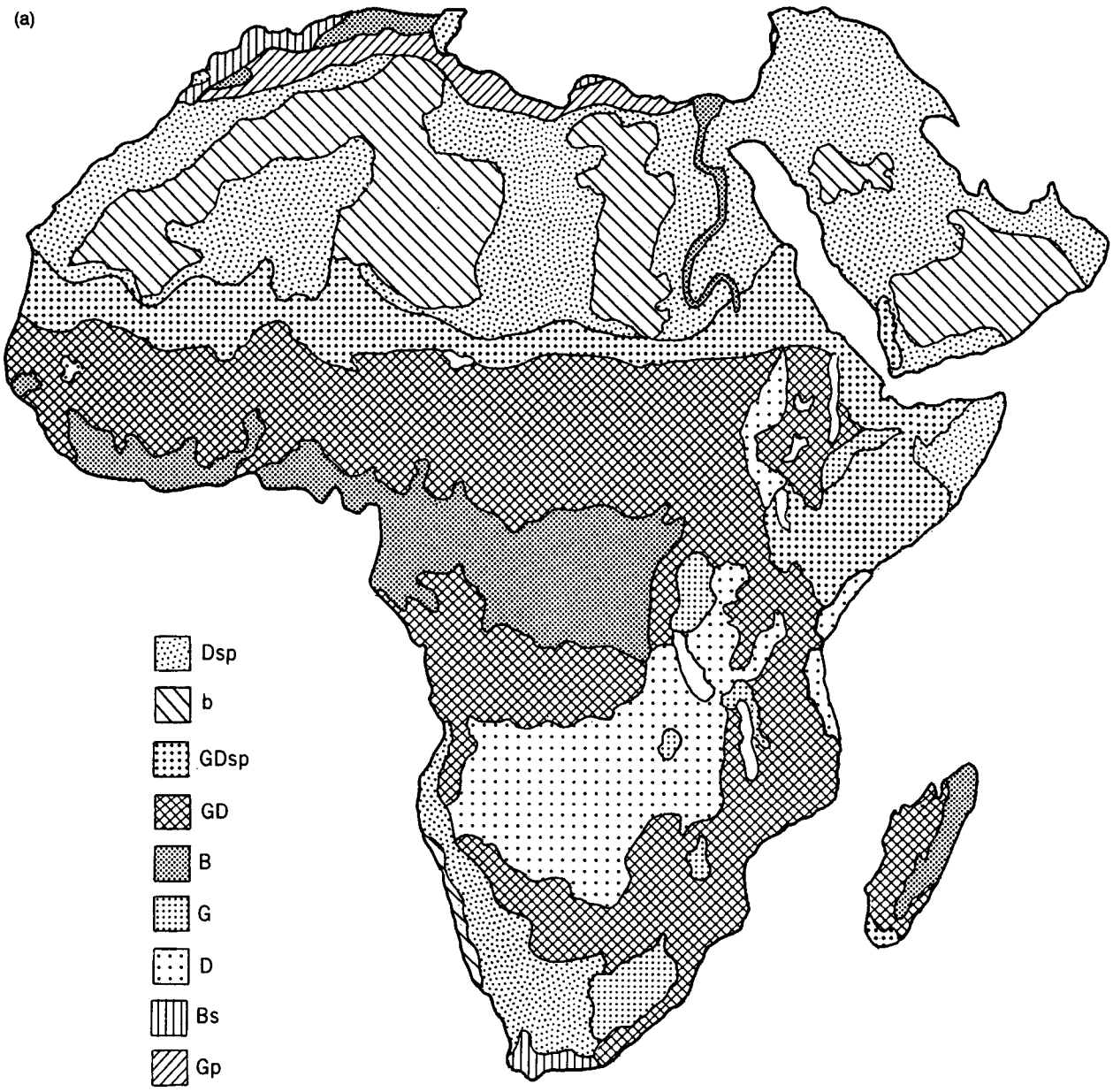

FIG. 2. (a) Reproduction of the African portion of the natural vegetation map of Küchler (1991). The abbreviations are as follows: Dsp, scattered broad-leaved deciduous dwarf shrubs; b, barren; GDsp, grassland with scattered broad-leaved deciduous shrubs; GD, grassland with scattered broad-leaved deciduous trees; B, broad-leaved evergreen forest; G, grassland; D, broad-leaved deciduous forest; Bs, broad-leaved evergreen shrub formation; and Gp, patches of grass. Map from The New International World Atlas, @ 1994 by Rand McNally, R. L. 94-S-206. (b) Classification of vegetation types in Africa derived by applying the generalized life zone scheme of Henderson-Sellers (1990) to observed precipitation data of Legates and Willmott (1990) and surface air temperature data of Oort (1983).

run at rhomboidal-30 resolution, in which surface albedo was held spatially invariant at a value of 0.17 over all snow-free land surfaces. The control case run was allowed to spin up for 3 yr, and the following 10-yr data was retained for analysis.

Predicting the surface albedo of the climax vegetation, given the climate of this control case, yields a spatially varying distribution $[S_1(x, y)]$. The difference between S_1 and the value prescribed for the control case (S_0) is labeled "initial change." Although it is schematically shown as an increase, it is a decrease in many places.

The distribution $S_1(x, y)$ of surface albedo is used as the initial condition for the experimental run, referred to as the ISA (interactive surface albedo) case. The experimental run was carried out at rhomboidal-

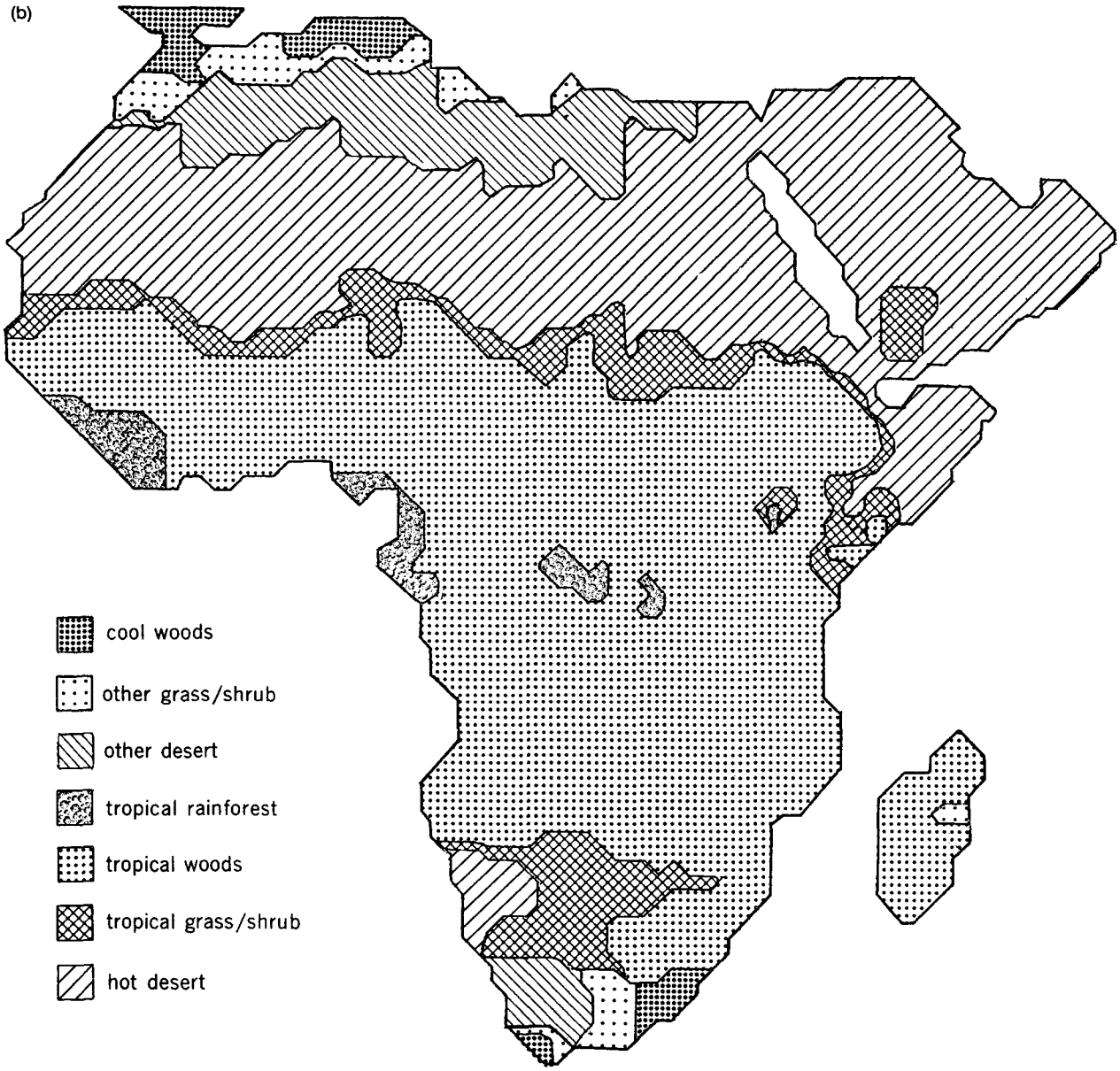

FIG. 2. (*Continued*)

30 resolution, and following each year of simulation, a new, slightly different surface albedo distribution was determined using the climate of the previous 5 yr. This process was continued until it was subjectively determined from inspection of maps of the time series of distributions that there was no longer a trend in the surface albedo values in each region, but only fluctuations (15 yr). Following this, the simulation was run for an additional 10 yr, from which the data was retained for analysis.

If the change in surface albedo from S_0 to S_1 results in a change in climate from the control case with spatially homogeneous surface albedo, it may cause a further change in surface albedo, from S_1 to S_2. In the example of Fig. 4, the further change $(S_2 - S_1)$ has the same sign as the initial change $(S_1 - S_0)$, indicating positive feedback. If the initial change and further change are of opposite sign, it indicates negative feedback.

Soil moisture will be used as another measure of aridity. Changes in soil moisture can be interpreted using a modified version of the analysis of initial and further changes in the surface albedo. The difference, in the control case, between the local mean and the global mean of the soil moisture (which will be referred to as the "initial anomaly") is analogous to the initial

TABLE 1. Approximate correspondences between classification schemes of Henderson-Sellers (1990) and Küchler (1982).

Henderson-Sellers classification	Küchler classifications
Desert (1, 2)	Scattered broad-leaved evergreen dwarf shrubs
	Broad-leaved deciduous shrub formation
	Scattered broad-leaved deciduous shrubs
	Scattered broad-leaved deciduous dwarf shrubs
	Patches of grass
	Barren
Grassland (3, 4)	Scattered broad-leaved evergreen shrubs
	Grassland with broad-leaved evergreen shrubs
	Grassland with broad-leaved deciduous shrubs
	Grassland
Woods (5, 6)	Broad-leaved evergreen shrub formation
	Broad-leaved deciduous forest
	Needle-leaved evergreen forest
	Needle-leaved deciduous forest
	Forest of broad-leaved evergreen and deciduous trees
	Forest of broad-leaved and needle-leaved evergreen shrubs
	Broad-leaved deciduous forests with broad-leaved evergreen shrubs
	Forest of broad-leaved deciduous and needle-leaved evergreen trees
	Grassland with scattered broad-leaved evergreen trees
	Grassland with scattered broad-leaved deciduous trees
Rainforest (7, 8)	Broad-leaved evergreen forest
Tundra (9)	Needle-leaved deciduous forest
	Lichens and grasses
	Lichens and mosses
	Barren

TABLE 2. Assumed correspondence between classification schemes of Henderson-Sellers (1990) and SiB (Dorman and Sellers 1989).

	Henderson-Sellers classification	Dorman and Sellers (SiB) classification
1	Hot desert	Bare soil
2	Other desert	Deciduous shrubs with bare soil
3	Tropical grass/shrub	Groundcover
4	Other grass/shrub	Groundcover
5	Tropical woods	Broadleaf-deciduous
6	Cool woods	Broadleaf and needleleaf
7	Rainforest	Broadleaf-evergreen
8	Temperate rainforest	Broadleaf-evergreen
9	Tundra	Dwarf trees and shrubs with groundcover

changes in surface albedo, and the further change is the difference in soil moisture between the experimental and control cases. As shown in Fig. 3, the predicted albedo is quite insensitive to changes in temperature or potential evaporation, soil moisture is a variable that is more strongly affected by potential evaporation.

The 5-yr averaging period for determining surface albedo from climate is not to be interpreted as representing a timescale characteristic of temporal variations in vegetation, but rather as a reasonable ensemble from which to derive the model's mean precipitation and biotemperature, with the goal of reaching a state in which the vegetation distribution is in equilibrium with the model-simulated climate. Because many regions in this GCM have grid-scale spatial variations in precipitation as permanent features, a simple 1-2-1 spatial smoothing is applied in two dimensions to the annual mean precipitation field before calculating the predicted surface albedo.

Although 0.17 was chosen as the homogeneous value of surface albedo for the control case because it is near the average value of surface albedo predicted by our scheme, it is still arbitrary, and it is assumed that the sign of any feedback discovered will be robust to the choice of control case conditions. Some test of this assumption will be made in subsection 4e, where comparison is made with an alternative control case with a constant land surface albedo of 0.25.

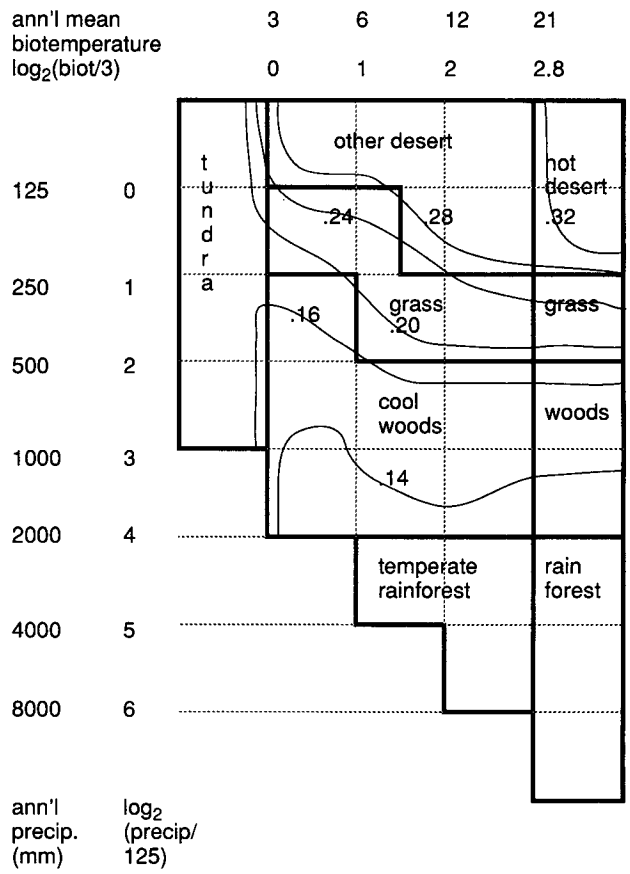

FIG. 3. Predicted values of surface albedo shown on a rectangular log–log plane with annual mean precipitation as the vertical coordinate and annual mean biotemperature as the horizontal coordinate.

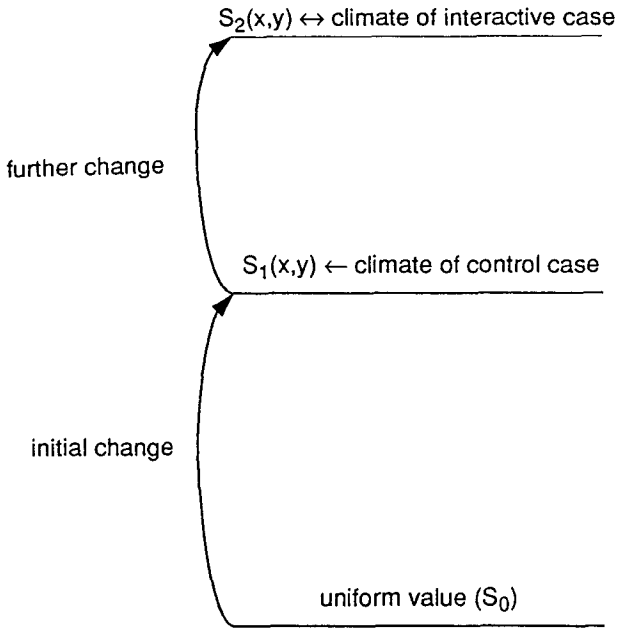

FIG. 4. Schematic diagram of feedback of surface albedo. A local surface parameter value S_1 is predicted using the climate of the control case. Another value of the surface parameter S_2 is predicted using the climate of the interactive case. The "further change" is due to feedback.

Because at some grid points, the initial change ($S_1 - S_0$, see Fig. 4) in surface albedo is near zero, it is not meaningful to calculate the ratio of further change to initial change, $(S_2 - S_1)/(S_1 - S_0)$ in individual grid boxes. Also, it is desirable to have variables areally averaged over regions representing various climatic regimes. Chosen regions are shown in Fig. 5. Region 1, central Africa, represents low-latitude forested regions; region 2, northern Africa, represents subtropical deserts; region 3, the Central Asian and Gobi Deserts, represents midlatitude deserts; region 4, eastern North America, is representative of midlatitude forested regions.

4. Model results

a. Generalized life zone classifications

Figure 6 shows the distributions of vegetation predicted using the climate from the GCM. Figure 6a shows the distribution predicted using the climate of the control case, and Fig. 6b shows the results from the ISA case. Although these two distributions are qualitatively similar, a closer examination reveals differences in detail.

Midlatitude distributions of vegetation are well represented. The woods classification covers most of North America and the eastern and western parts of Eurasia. The desert classification appears over a large region representing the Gobi and Central Asian Deserts and over a smaller region in southwestern North America. These deserts are bordered by grassland.

At lower latitudes, however, both deserts and rainforests are underrepresented, with low-latitude continents dominated by the woods classification. The control case of the model (Fig. 6a) does not have sufficient precipitation to produce rainforests in more than a few grid boxes in the Amazon Basin. This is partially remedied in the ISA case (Fig. 6b). The GCM produces excessive precipitation over topographic features in eastern Africa and Indochina, giving an exaggerated extent of rainforests in those places.

The deserts of northern and southwestern Africa and western Australia are unrealistically small. This problem is reduced in the ISA case, with subtropical deserts

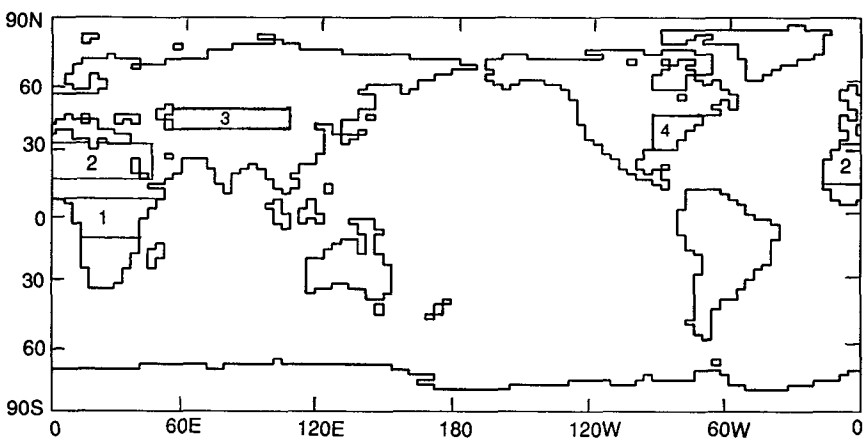

FIG. 5. Geographical regions that will be used for subsequent analysis. Region 1 will be known as central Africa; region 2, northern Africa; region 3, Central Asian and Gobi Deserts; and region 4, eastern North America.

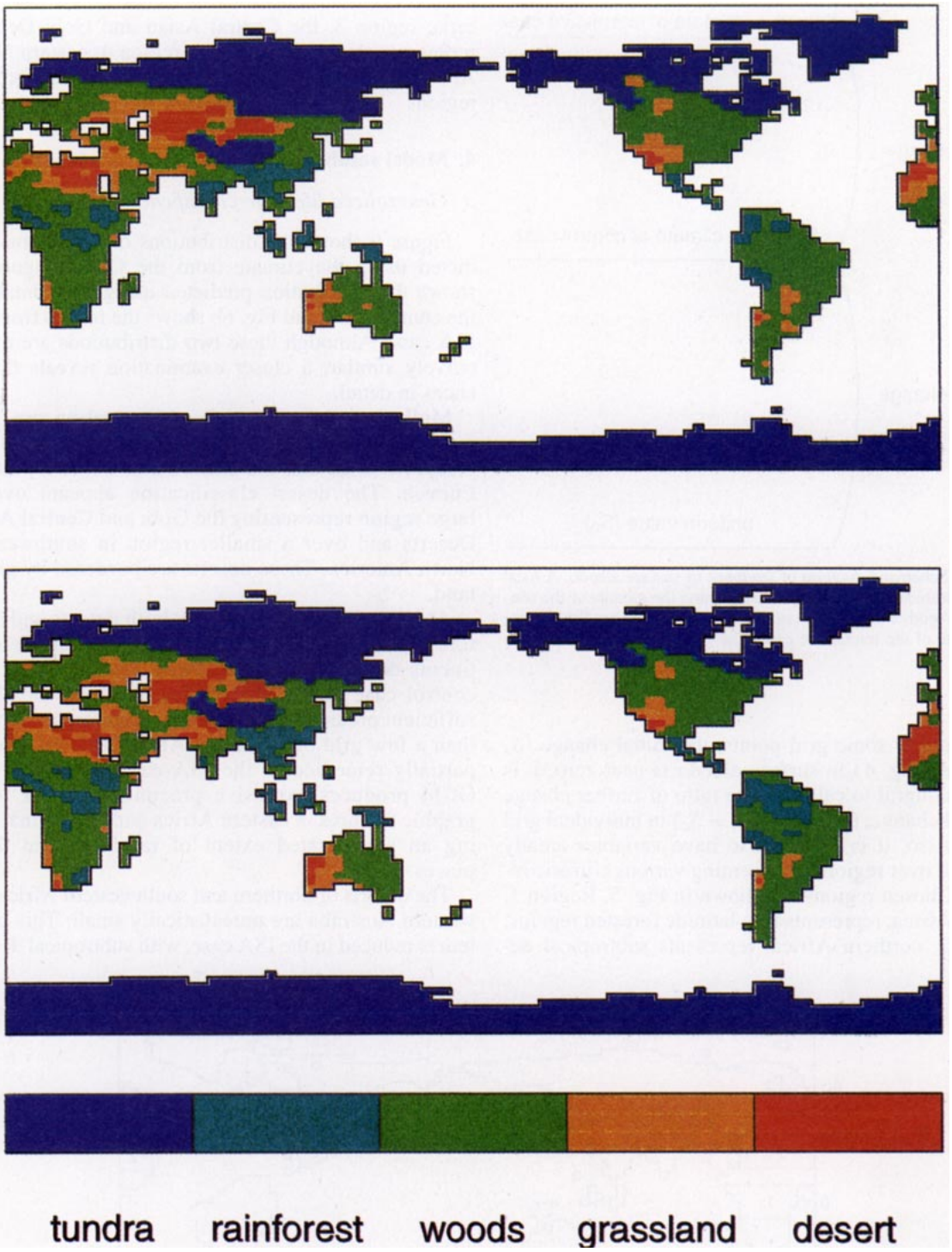

FIG. 6. Vegetation types predicted by the scheme of Henderson-Sellers (1990) (see Fig. 1) using the climate of (a) the control case and (b) the ISA case. For the purposes of this figure, the distinction made by Henderson-Sellers between tropical and cool vegetation types has been suppressed.

expanded, especially in northwestern Africa, and the grassland region in Australia also expanded, pushing back the region classified as woods. Overall, the vegetation predicted using the climate of the ISA case is closer to realistic natural vegetation than that using the climate of the control case.

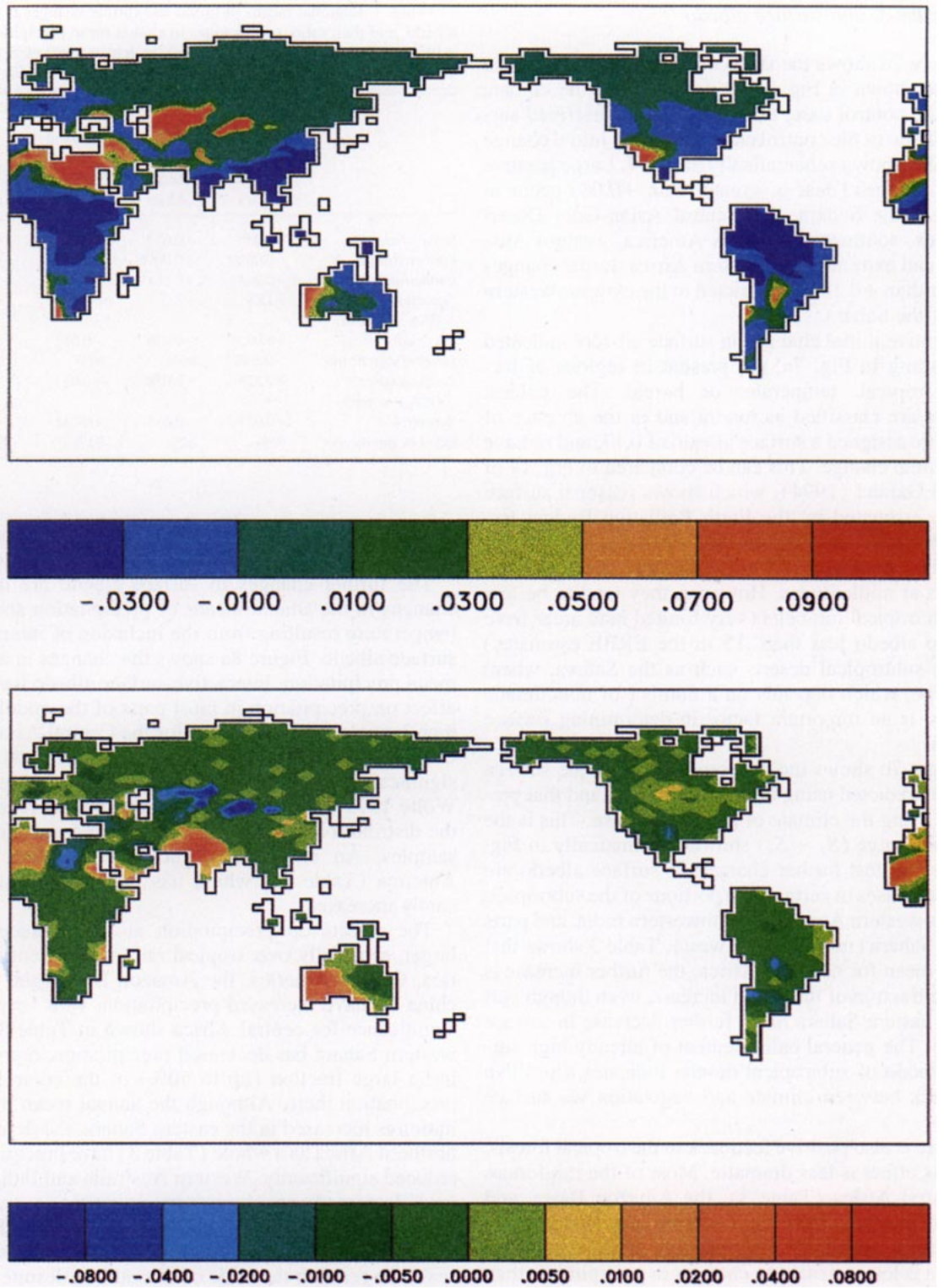

FIG. 7. (a) Snow-free surface albedo predicted using the climate of the control case, minus 0.17. (b) Snow-free surface albedo predicted using the interactive surface albedo case climate minus that predicted using the control case climate.

b. *Feedback into surface albedo*

Figure 7a shows the surface albedo predicted by the scheme shown in Fig. 3, when applied to the climate from the control case, minus 0.17, the prescribed surface albedo of the control case. This is the initial change ($S_1 - S_0$) shown schematically in Fig. 4. Large positive initial changes (near or greater than +0.08) occur in deserts—the Sahara, the Central Asian-Gobi Desert complex, southwestern North America, western Australia, and extreme southwestern Africa. Initial changes greater than +0.12 are restricted to the extreme western part of the Sahara.

Negative initial changes in surface albedo, indicated by shading in Fig. 7a, are present in regions of forests—tropical, temperate, or boreal. The coldest regions are classified as tundra and in the absence of snow are assigned a surface albedo of 0.17, and so have zero initial change. This can be compared to Fig. 14 of Li and Garand (1994), which shows seasonal surface albedo estimated by the Earth Radiation Budget Experiment (ERBE). The surface albedo values used in this paper compare well to the summertime ERBE estimates at midlatitudes. However, they tend to be low in both tropical rainbelts (very limited land areas have surface albedo less than .15 in the ERBE estimates) and in subtropical deserts such as the Sahara, where soil type, which depends on a number of nonclimatic factors, is an important factor in determining surface albedo.

Figure 7b shows the difference between the surface albedo predicted using the climate of ISA and that predicted using the climate of the control case. This is the further change ($S_2 - S_1$) shown schematically in Fig. 4. The greatest further changes in surface albedo are large increases in certain arid portions of the subtropics, such as western Australia, northwestern India, and parts of the Sahara (mostly in the west). Table 3 shows that in the mean for northern Africa, the further increase is a large fraction of the initial increase, even though part of the eastern Sahara has a further decrease in surface albedo. The general enhancement of already high surface albedo of subtropical deserts indicates a positive feedback between climate and vegetation via surface albedo.

There is also positive feedback in the tropical forests, but this effect is less dramatic. Most of the rainforests of central Africa (Table 3), the Amazon Basin, and eastern Australia have their surface albedo decreased by modest amounts, since surface albedo in moist regions is less sensitive to changes in precipitation than in arid regions (Fig. 3).

In the Central Asian and Gobi Deserts, the ratio of further change to initial change in surface albedo (Table 3) indicates a modest negative feedback, while eastern North America shows an apparent positive feedback of similar strength. On the whole, however, the patterns of further change in midlatitudes are not well correlated with the initial change in surface albedo.

TABLE 3. Regional means of initial and further changes in surface albedo, and their ratio, and changes in annual mean precipitation (in millimeters per year) and soil moisture (in centimeters), with ratio to their control case values. For the location of regions, see Fig. 5.

	1. Central Africa	2. Northern Africa	3. Central Asian and Gobi Deserts	4. Eastern North America
Initial change	−0.035	+0.053	+0.088	−0.023
Further change	−0.0005	+0.0096	−0.0041	−0.0013
Further/initial	+0.014	+0.181	−0.046	+0.056
Δprecipitation (ISA − control)	+13.8	−3.2	−0.3	+5.2
Δ/control	+0.083	−0.076	−0.012	+0.054
Level of significance	>99.9%	99%	59%	99%
Δsoil moisture (ISA − control)	+0.228	−0.038	+0.093	+0.127
Δ/control	+0.037	−0.034	+0.081	+0.017
Level of significance	90%	82%	92%	92%

The further changes in surface albedo are due to changes in the annual means of precipitation and biotemperature resulting from the inclusion of interactive surface albedo. Figure 8a shows the changes in annual mean precipitation. Interactive surface albedo has little effect on precipitation in most parts of the middle and high latitudes. This is shown for the Central Asian and Gobi Deserts in Table 3, with measures of statistical significance using the Wilcoxen test (Hollander and Wolfe 1973), which makes no assumptions regarding the distribution of sampled results or independence of samples. An exception occurs over eastern North America (Table 3), which has precipitation significantly increased.

The effects on precipitation at low latitudes are larger, especially over tropical rainforests. Central Africa, Central America, the Amazon Basin, and Indochina all have increased precipitation, with very high significance for central Africa shown in Table 3. The western Sahara has decreased precipitation, representing a large fraction (up to 50%) of the control case precipitation there. Although the annual mean precipitation is increased in the eastern Sahara, the deserts of northern Africa as a whole (Table 3) have precipitation reduced significantly. Western Australia and India also have decreased annual mean precipitation.

Several figures in this paper, including Fig. 8, use spatial smoothing to extract information at spatial scales larger than the scale of smoothing, despite computational noise at the scale of finest resolution. Precipitation is a particularly noisy field, with time-averaged values on adjacent grid boxes differing by factors up to approximately 5, particularly in the vicinity of isolated topographic features, such as the Himalayas, Central America, and the Indonesian islands.

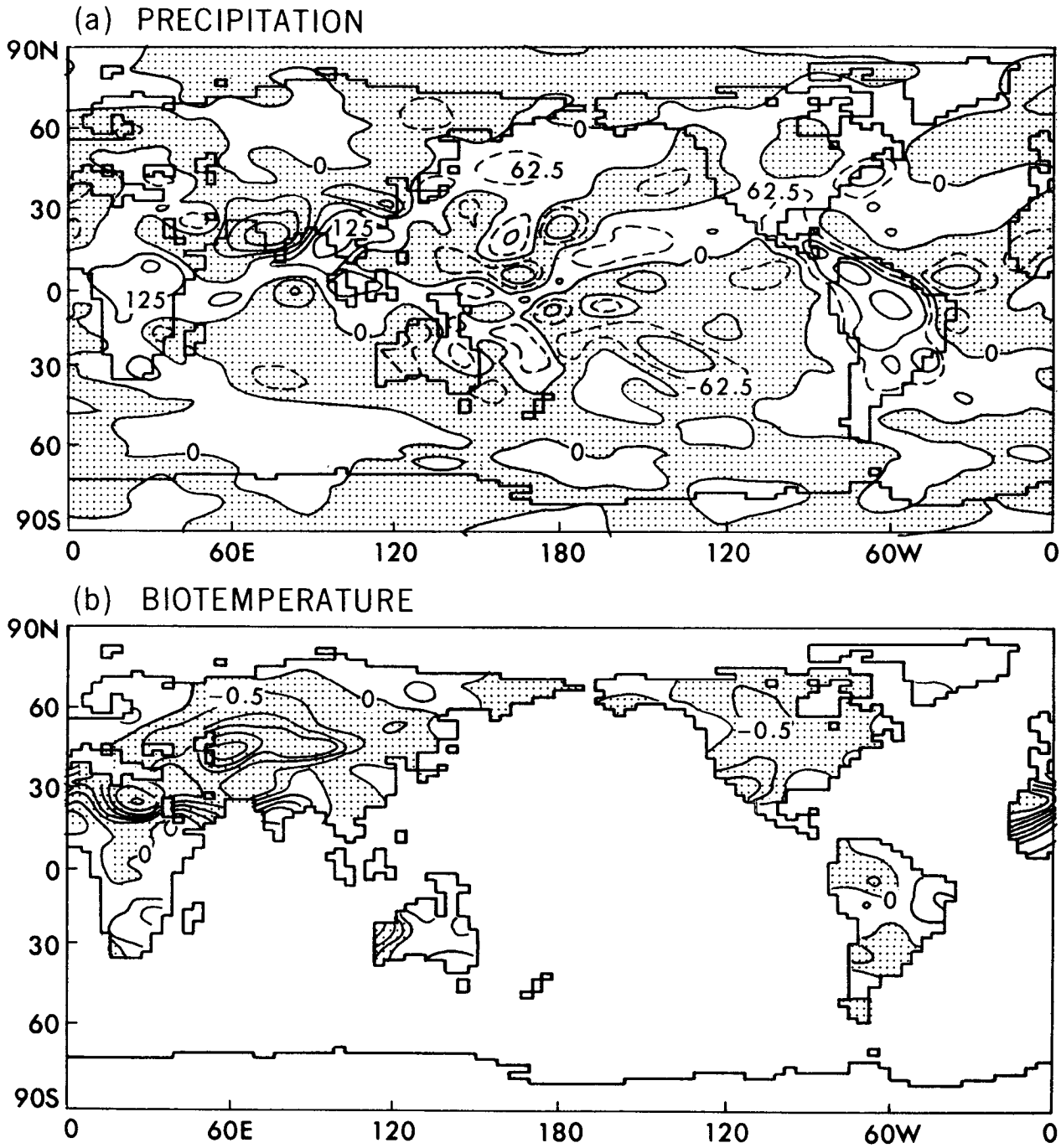

FIG. 8. Annual means for ISA minus the control case of (a) precipitation (in millimeters per year) and (b) biotemperature (in degrees Celsius). To suppress noise near the scale of the grid, a 1-4-6-4-1 spatial smoothing was applied to both fields. In part (a), the contours are 0, ±62.5, 125, 250, and 500. In part (b), the contour interval is 0.5. Shading indicates negative values.

The changes in annual mean biotemperature (Fig. 8b) share many features in common with the distribution of initial change in surface albedo (Fig. 7a). However, other factors, mainly the precipitation rate, also influence the biotemperature. Therefore, although most low albedo areas have increased annual mean biotemperature due to interactive surface albedo, most of North America has a decrease, along with part of the Amazon Basin, Indochina, and central Africa, and some wooded parts of Siberia, all of which have increased precipitation. The increase in biotemperature in India due to decreased surface albedo is amplified

by the lack of precipitation. In western Australia, because of decreased precipitation, the region of decreased biotemperature is considerably smaller than the region with initially increased surface albedo.

Figure 9 shows the initial anomaly and further change in annual mean soil moisture over most of Africa, Europe, and Asia. In central Africa and Indochina, where the initial anomaly is positive, soil moisture is further increased due to increased precipitation, indicating positive feedback. In the Sahara and India, where the initial soil moisture anomaly is negative, precipitation and soil moisture are decreased, again a positive feedback. Despite the high statistical significance of the changes in precipitation in these regions (Table 3), the significance levels of these changes in soil moisture are more marginal.

Along the northern edge of Africa and throughout most of Europe and Asia, there are smaller changes in precipitation (Fig. 8a), and the reduction of potential evaporation due to their high albedo is dominant, al-

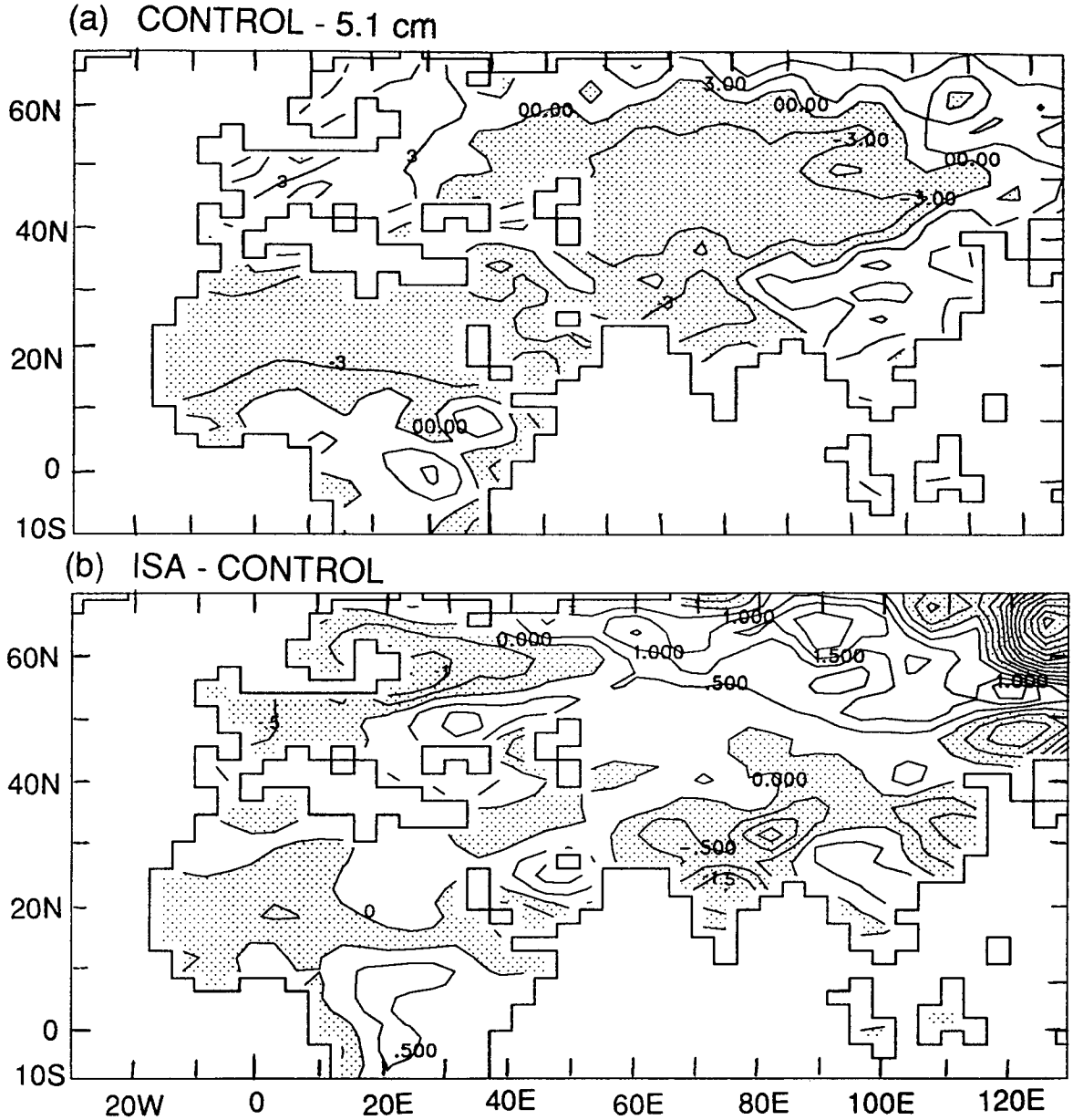

FIG. 9. Annual mean soil moisture (in centimeters) for (a) the control case, with 5.1 cm subtracted, and (b) ISA minus the control case. To suppress grid-scale noise, a 1-2-1 spatial smoothing has been applied to this data. Contour interval for part (a) is 3, for part (b), 0.5.

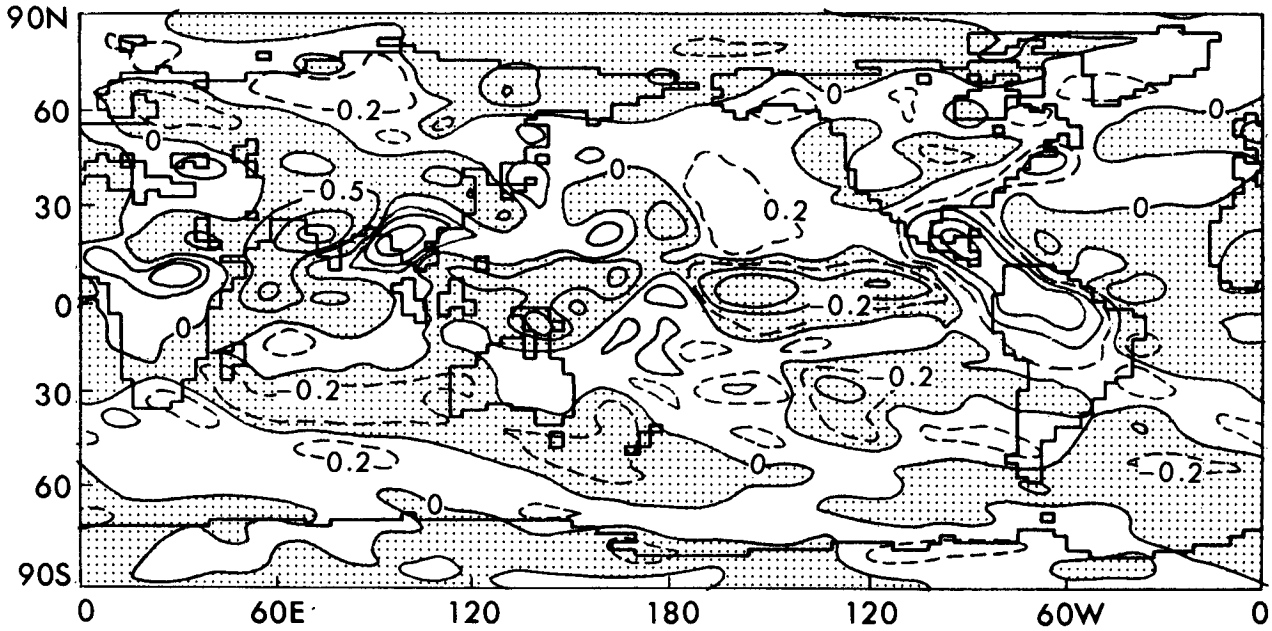

FIG. 10. Precipitation (in millimeters per day) during JJA for ISA minus the control case. Smoothing as in Fig. 8. Solid contours represent 0, ±0.5, 1, 2, and 5. Dashed contours represent ±0.2 but have been omitted in some places for clarity.

lowing the soil to retain more moisture. This increased soil moisture on the northern edge of the Sahara, coupled with the decrease in soil moisture farther south, implies a southward shift of the Sahara. Soil moisture is also increased in the Central Asian and Gobi Deserts. The initial anomaly of soil moisture in these places is negative, so this indicates a negative feedback. The increase in soil moisture over the Central Asian and Gobi Deserts (Table 3) is 8.1%, a larger percentage change than in any of the other selected regions.

Soil moisture is decreased in the forests of Europe and eastern Asia. Since there is a positive initial anomaly in soil moisture, this indicates negative feedback. In contrast, the small initial decrease in surface albedo over eastern North America (Table 3) does not produce a large enough change in potential evaporation to offset the increased precipitation, so soil moisture is increased there, implying a positive feedback. In Siberia, the small insolation limits the influence of surface albedo, and small changes in precipitation can have large effects on soil moisture.

c. *Climate during June, July, and August*

The direct effect of a change in surface albedo is to modify the amount of sunlight that is absorbed at the ground. Although this change in solar heating of the ground is partially compensated by a change in the outgoing longwave flux from the ground, the net radiative heating of the surface (not shown) is reduced in case ISA over the high-albedo deserts (by up to 20% of its control case value in parts of the Sahara) and increased in forested regions. The increase in net radiative heating in forested regions is small in the tropical rainbelts, where increased clouds moderate the net radiative forcing. Also, because the surface albedo of forests departs from the control case value of 0.17 by smaller amounts than in the deserts, their net radiative heating is changed by smaller amounts.

Associated with these changes in net radiative heating of the surface are changes in precipitation. Figure 10 shows the precipitation during June, July, and August (JJA) for ISA minus the control case. The largest changes in precipitation are increases in Northern Hemisphere regions near the Tropics, where precipitation is normally greatest during this season, including the African summer monsoon rainbelt (in the vicinity of 10°N), the Indochinese monsoon region, Central America, and the northern Amazon Basin, all of which have initial decreases in surface albedo. These increases in precipitation are in the range of 10%–20% of the control case's JJA precipitation.

However, there are a couple of notable exceptions to the general rule of initially decreased albedo at low latitudes in the summer hemisphere yielding increased precipitation. Although the surface albedo is initially decreased in most of India, its summertime precipitation is decreased in case ISA. Analysis of water vapor flux vectors (not shown) shows that water vapor from the Indian Ocean moves more toward the Indochinese region, which has even lower surface albedo. Similarly, the western part of the African monsoon region, with initially decreased surface albedo, forfeits its water vapor to regions farther east, with lower surface albedo.

The changes in precipitation in the Sahara and Arabian Deserts are varied. There are strong decreases in precipitation in the western Sahara and near the Red Sea, especially when considered as a fraction of the precipitation in the control case (some areas in the western Sahara have a 50% decrease). However, there is increased precipitation in northeastern Africa. There is an overall decrease in precipitation for the northern Africa region (Fig. 5), but this variation within this region is unexplained.

The mechanisms leading to these changes in precipitation at low latitudes are similar to those explained in Lofgren (1995). That is, changes in local evaporation have some influence on precipitation, but changes in the horizontal convergence of water vapor due to thermally forced motion play a larger role. JJA precipitation minus evaporation is displayed in Fig. 11 for ISA minus the control case, and is nearly equal to the vertically integrated convergence of water vapor in the atmosphere. When compared with Fig. 7a, this shows a general pattern of increased water vapor flux convergence where initially decreased albedo yields thermally forced ascent (the African rainbelt, Indochina, and Central and South America), and decreased water vapor flux convergence where initially increased albedo yields relative descent (the Sahara and Kalahari Deserts).

Figures 10 and 11 indicate that in middle and high latitudes the changes in precipitation and water vapor flux convergence are considerably smaller than those in the Tropics and subtropics. However, the changes in precipitation over eastern North America have high statistical significance (Table 3). Comparison with the map of initial change in surface albedo (Fig. 7a) also shows that there is no obvious spatial correlation at middle and high latitudes between the changes in precipitation and the initial changes in surface albedo.

Figure 12 displays the vertical p-velocity, zonally averaged over land only in the range of longitudes encompassing Africa (15°W to 52.5°E) and illustrates the vertical motion associated with water vapor flux convergence over Africa, characterized by zonal bands of upward and downward motion (which shift with season) and by zonal bands of surface albedo. During the Northern Hemisphere summer in the control case (Fig. 12a), the Hadley cell over Africa is asymmetric about the equator. Ascending motion occurs north of the equator, in a band centered near 15°N. This intense rising motion is partially compensated by a broad region of sinking to its south. Additional downward motion occurs over neighboring oceans.

Away from the surface at low latitudes, this vertical velocity is such that it yields adiabatic cooling to approximately balance the diabatic heating, shown in Fig. 13 (see Held 1985). In the control case (Fig. 13a), there is diabatic heating near the surface throughout all of the illustrated latitudes. However, over the deserts, this heating is shallow and does not result in deep enough rising motion to produce convective condensation. At middle- and upper-tropospheric levels outside of the rainbelt, radiative cooling of the atmosphere

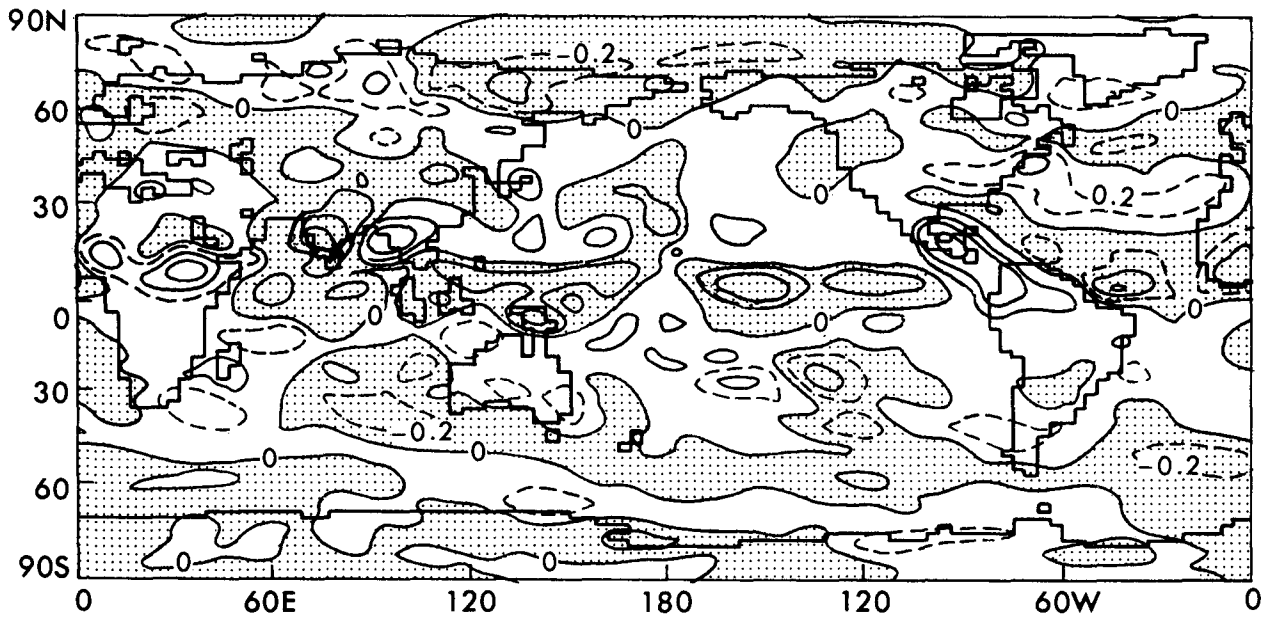

FIG. 11. JJA map of precipitation minus evaporation (mm day^{-1}) for ISA minus the control case. Smoothing as in Fig. 8. Contours as in Fig. 10.

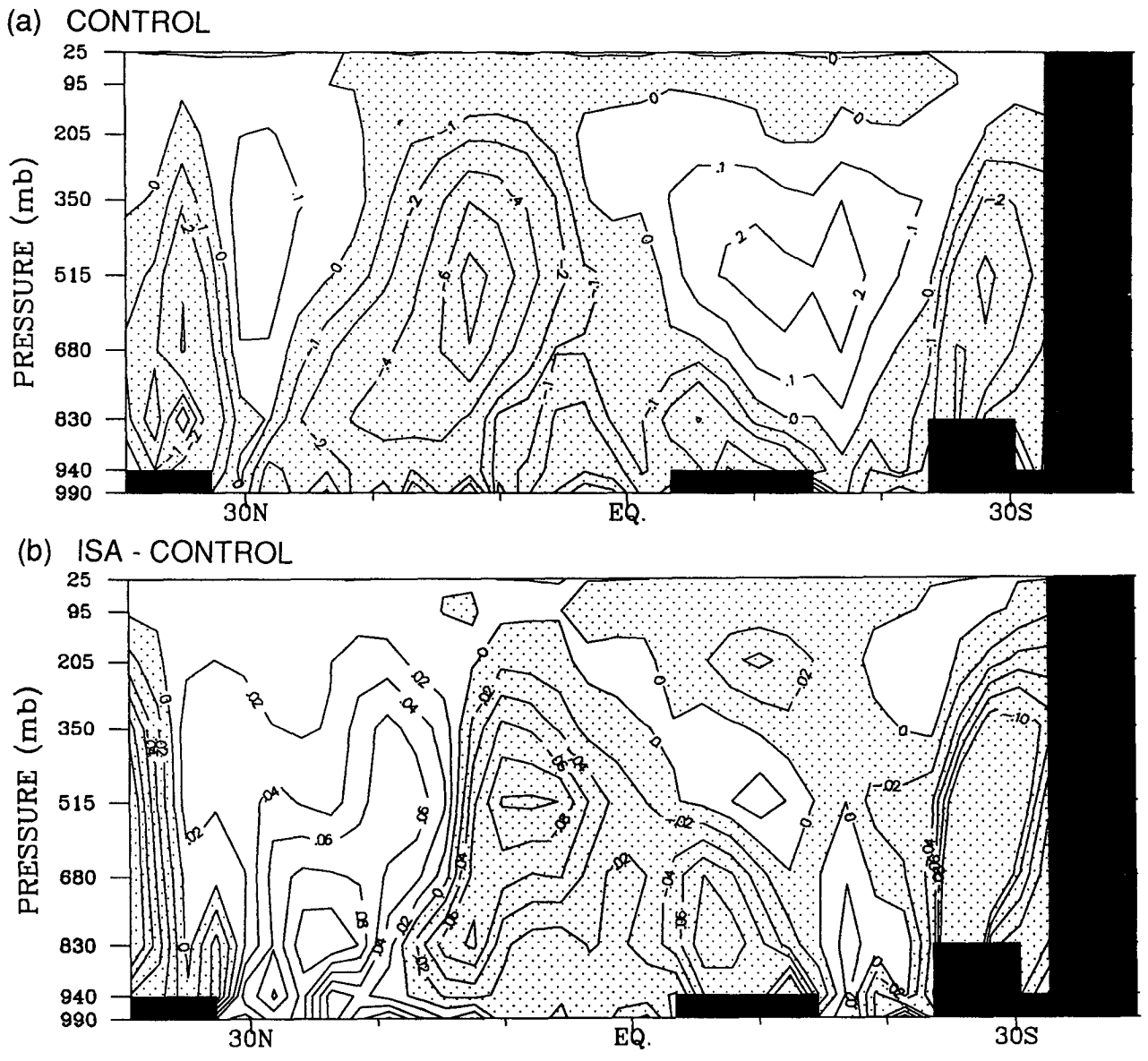

FIG. 12. JJA latitude vs height cross sections of vertical p-velocity (μbar s^{-1}), zonally averaged over land in the range 15°W to 52.5°E (corresponding to Africa) for (a) the control case and (b) ISA minus the control case.

dominates over condensational heating, giving net diabatic cooling, accounting for the broad regions of slow sinking motion shown in Fig. 12a. The release of latent heat from convective condensation along the rainbelt (centered near 10°N) extends through a much greater depth and corresponds with the maximum of upward motion. Therefore, this diabatic heating feeds back on itself; the resulting upward motion means that moist air is converging at low levels and promoting convective condensation, releasing latent heat for further diabatic heating.

The inclusion of interactive surface albedo creates a contrast between the high albedo of the deserts and the low albedo of the forests of central Africa, which leads to changes in diabatic heating. During JJA, when insolation is greater in the Northern Hemisphere, it is expected that these changes in surface albedo will have the greatest effect in the Northern Hemisphere, as confirmed by Figs. 12b and 13b. The initial decrease in surface albedo in central Africa generally causes increased diabatic heating near the surface due to increased sensible heat flux, and at midtropospheric levels due to latent heat release from condensation of water vapor, both from local evaporation and from convergence of water vapor originating elsewhere. This leads to both an intensification and a southward shift

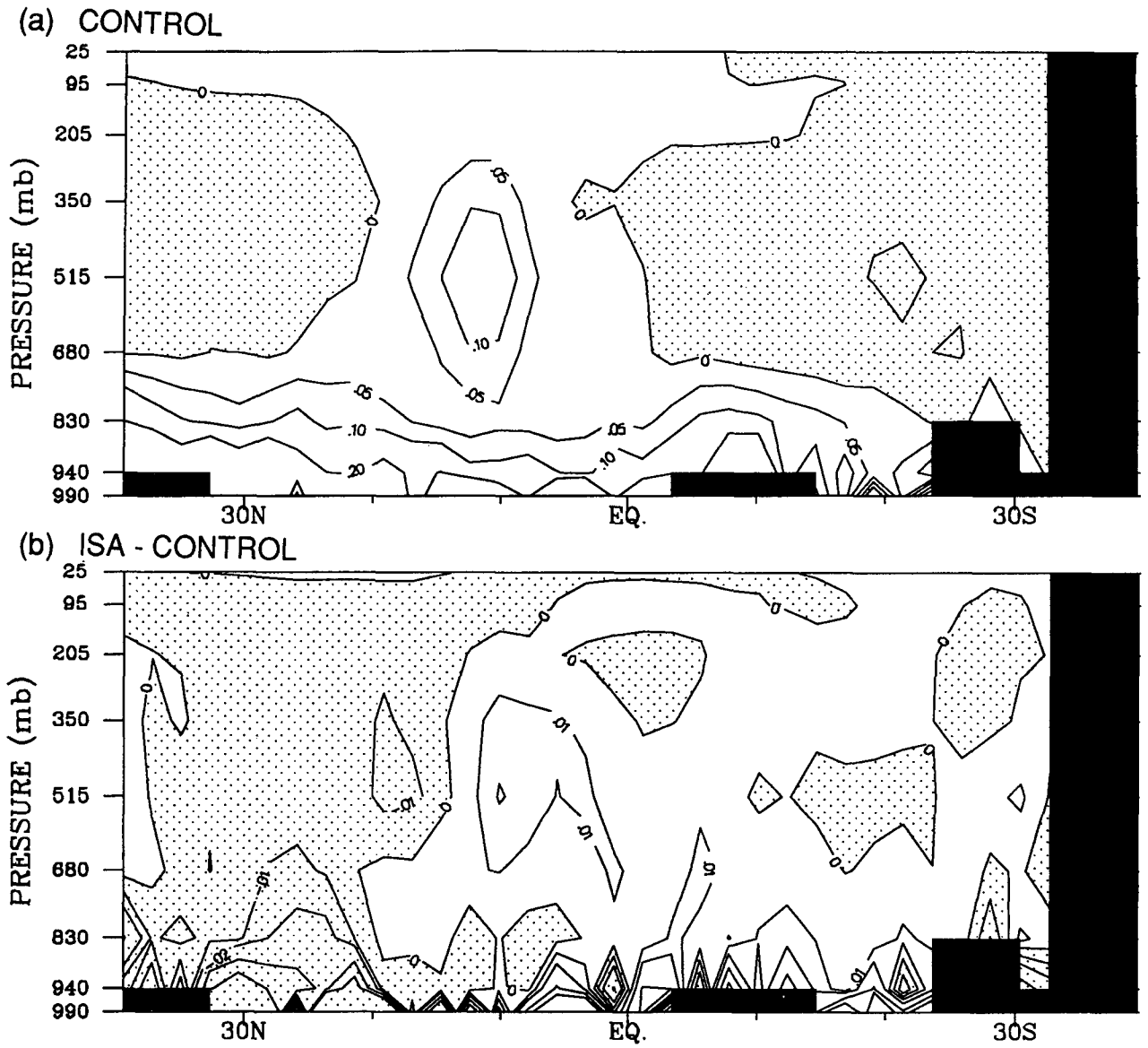

FIG. 13. JJA latitude vs height cross sections of diabatic heating (K h^{-1}), zonally averaged over land in the range 15°W to 52.5°E (corresponding to Africa) for (a) the control case and (b) ISA minus the control case.

(toward the rainforests) of the upward branch of the Hadley cell during JJA.

In the reverse of this, the initial increase in surface albedo of northern Africa causes relative diabatic cooling and intensifies the downward motion over northern Africa. Because the relative diabatic cooling over the Sahara is primarily due to decreased sensible heat flux, it and the associated downward motion occur most strongly at low levels. The effects of initially increased surface albedo on the vertical motion over southern Africa during JJA are much weaker, both because the insolation there is less and because the surface albedo there is initially increased by a smaller amount than in northern Africa.

d. Climate during December, January, and February

During December, January, and February (DJF), the Southern Hemisphere summer, the responses in precipitation (Fig. 14) show the same characteristics as those during JJA; the regions of greatest response are along the rainbelts, which have migrated into the Southern Hemisphere. Instead of being located along an axis near 10°N, as it was during JJA, Africa's region of increased precipitation extends approximately from the equator to 25°S, except near the western coast, where an initial increase in surface albedo is present over a small desert region, and precipitation is reduced there.

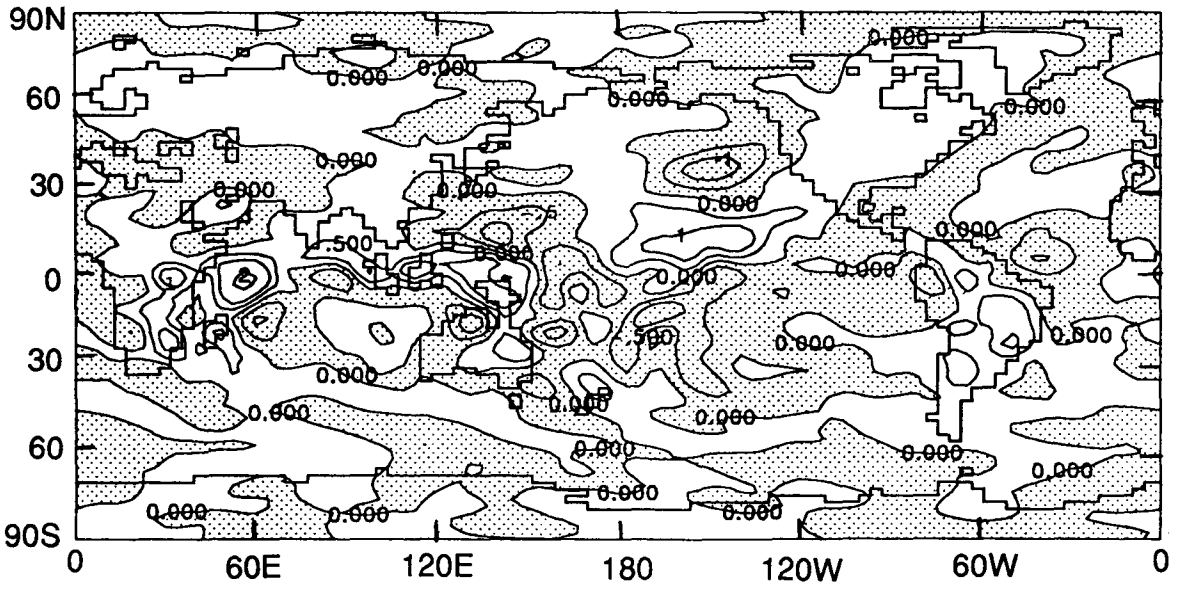

FIG. 14. DJF precipitation (mm day^{-1}) for ISA minus the control case. Smoothing as in Fig. 8. Contours as in Fig. 10.

The pattern is maintained in which low-latitude regions with initially decreased surface albedo, such as Indonesia and eastern Australia, have increased precipitation. In South America, DJF precipitation is increased most strongly in southern Brazil, the location of the seasonal rainbelt. There are (usually smaller) decreases in precipitation in low-latitude areas where there is an initial increase in surface albedo, such as the desert of western Australia. During DJF, as in JJA, there is little discernible correlation between precipitation changes and surface albedo in the midlatitudes.

e. Alternate control case with high surface albedo

The value of land surface albedo used in the control case, 0.17, although it yields approximately the same globally averaged solar absorption at the ground as the ISA case, is an arbitrary reference level. The minimum value of land surface albedo in our prediction scheme is 0.13 (Fig. 3), which is much closer to the "average" value than is the maximum, 0.33. This means that arid regions, in which surface albedo is increased by up to 0.16, are more strongly forced than forests, in which surface albedo is lowered by no more than 0.04. For this reason, an additional control run was made to enhance the contrast in the surface albedo of forests between the control case and the interactive case, in order to better highlight the response to initially decreased surface albedo. This alternate control case, called Con25, has a constant land surface albedo of 0.25 where there is no snow, so that it has high contrast with forests and low contrast with deserts. It was run at rhomboidal-30 resolution and 7 yr of data were retained after a 2-yr spinup period.

The Con25 case is compared here with the same ISA case as was the control case with surface albedo of 0.17. Unlike the former control case, the absorbed solar radiation at the surface is significantly lower in Con25 than in ISA. Averaged over land only, absorbed solar radiation is 212.5 W m^{-2} in ISA and 203.5 W m^{-2} in Con25, or 4.2% less. Averaged over the entire globe, it is 1.6% less.

When comparing the ISA case with Con25, the surface albedo is initially decreased except in small regions (Fig. 15a). This leads to a general increase in precipitation (not shown) at low latitudes, even in most of the regions where there is an initial increase in surface albedo. This causes further changes in surface albedo (Fig. 15b) to be negative over nearly all land of the Tropics and subtropics, indicating positive feedback, except in extreme western Australia and the southwestern corner of the Sahara, both of which have decreased annual mean precipitation. As in the comparison between ISA and the control case with surface albedo of 0.17 (Fig. 7b), the largest further changes in surface albedo occur in arid regions (Fig. 15b), with negative further changes in the Sahara, southern Africa, northeastern Australia, and northwestern India.

All of the middle and high latitudes, except for small regions in the Central Asian and Gobi Deserts and southwestern North America, have negative initial changes in surface albedo with respect to Con25, but their further changes (Fig. 15b) are mixed. The Central Asian Desert has small positive further changes, while southwestern North America has negative. Areas of the middle and high latitudes with initial decreases in surface albedo of varying amounts have precipitation

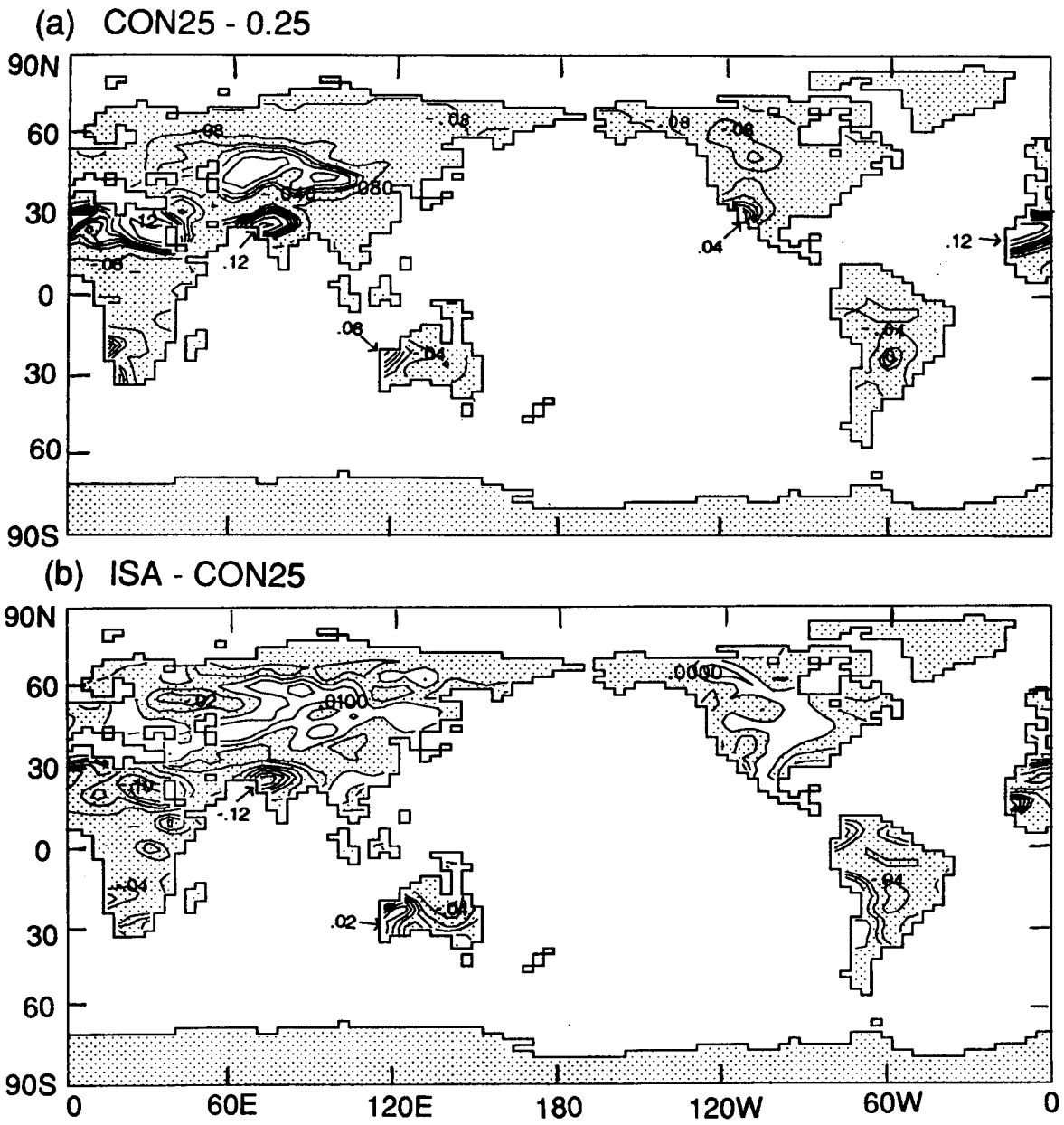

FIG. 15. (a) Snow-free surface albedo predicted using the climate of the Con25 case, minus 0.25. The contours are 0, ±0.02, 0.04, 0.08, and 0.12, and shading represents negative values. (b) Snow-free surface albedo predicted using the interactive surface albedo case climate minus that predicted using the Con25 case climate. Contours are 0, ±0.01, 0.02, 0.04, and 0.06. Smoothing as in Fig. 9.

changes of varying sign and, correspondingly, further changes in surface albedo of varying sign.

Soil moisture (Fig. 16) has a great distinction in its response between low and middle latitudes. Because the global mean soil moisture in the control case, 5.1 cm, is inconsistent with the surface albedo value that was used in the Con25 case, the concept of initial anomalies in soil moisture will not be invoked here. As a result of the increase in precipitation (not shown) when ISA is compared with Con25, annual mean soil moisture increases almost universally in the Tropics and subtropics. In contrast, Eurasia and North America have mainly decreased soil moisture because of the increased surface temperature and potential evaporation resulting from decreased surface albedo. A major exception exists in the area of very high surface albedo in the Central Asian and Gobi Deserts.

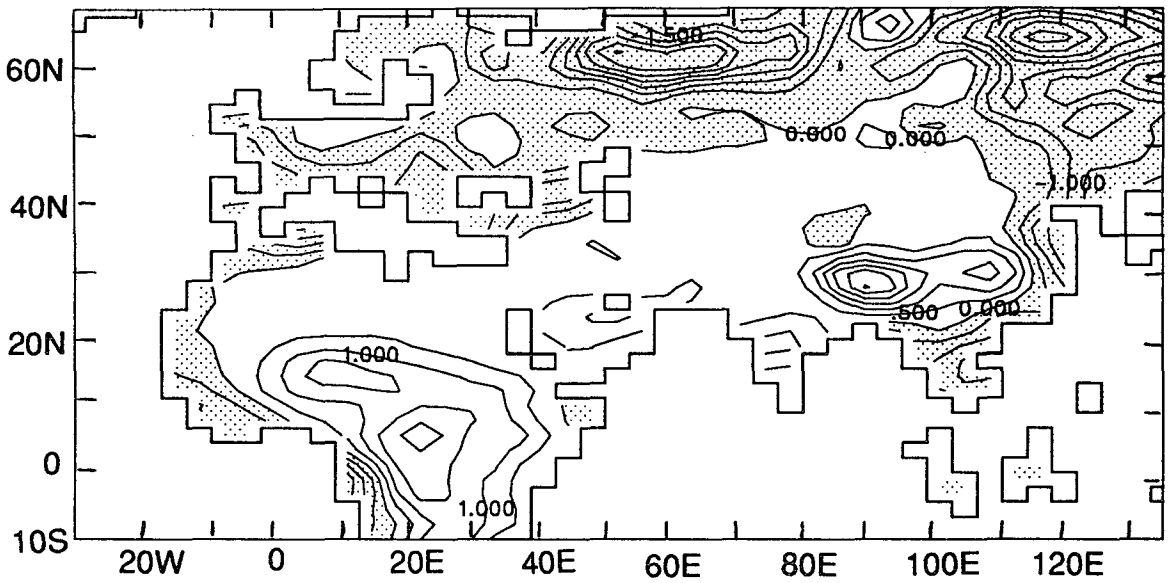

FIG. 16. Annual mean soil moisture for ISA minus the Con25 case (cm). Smoothing as in Fig. 9. Contour interval is 0.5.

5. Conclusions

GCM simulation experiments were carried out to determine the effects of land surface albedo on the simulated climate, and the way in which climate's effect on vegetation and surface albedo can lead to feedbacks. These feedbacks were investigated to see if they might play a role in enhancing or limiting the strength of features of the present general circulation and the resulting distribution of vegetation. Significant positive feedback between vegetation and climate via surface albedo has been demonstrated for low latitudes. Weaker negative feedback has been demonstrated for midlatitude deserts, and results for heavily vegetated midlatitude regions were inconclusive. These results were obtained by comparing an interactive GCM simulation, in which land surface albedo was made interactive with the simulated climate, to another simulation in which land surface albedo was prescribed to a spatially invariant value of 0.17.

In the interactive case, as in reality, subtropical deserts have surface albedo higher than 0.17. In qualitative agreement with the results from prescribed perturbations in surface albedo (Lofgren 1995), this increase in natural surface albedo leads to decreased precipitation in subtropical deserts because it thermally forces relative sinking motion. This precipitation decrease is of small absolute amplitude, but is a sizable fraction of the precipitation in the control case (typically around 10%–20%, in some places near 50%). Soil moisture is also generally decreased in subtropical deserts as a result. Thus, the high surface albedo associated with the dryness of subtropical deserts forces climatic effects that lead to further drying and sparser vegetation, further increasing the surface albedo, sustaining the deserts by this positive feedback mechanism. This is the same conclusion as that proposed by Charney (1975), but here is based on a model that includes the entire feedback loop.

Tropical rainforests, when made interactive with climate, have surface albedo lower than 0.17. The resulting increase in net radiative heating leads to rising atmospheric motion. The increased rising motion gives increased water vapor flux convergence, as in Sud and Smith's (1985) experiment with perturbed surface albedo over India. This enhanced water vapor flux convergence, along with increased latent heat flux from local sources, leads to increased precipitation and soil moisture, further increasing the vegetation and decreasing surface albedo. Thus, the rainforest also tends to sustain itself through positive feedback.

However, the positive feedback in rainforests is not as strong as in the deserts because surface albedo is near an asymptotically low value. In a forest, more precipitation may mean more trees and undergrowth, but this gives little change in the albedo of an already vegetated landscape. In a desert, a decrease in precipitation may result in the loss of what little vegetation there is and dramatically increase surface albedo.

Making surface albedo interactive with climate in the middle latitudes changes precipitation very little. However, when midlatitude deserts, such as the Central Asian and Gobi Deserts, are allowed to have high albedos consistent with their dryness, rather than 0.17, it lowers their surface temperature and potential evaporation. This allows them to retain more soil moisture; thus their high albedo acts to moderate their dryness, a negative feedback. In the opposite case, the low surface

albedo of midlatitude forests can lead to drying of the soil, but this effect is less consistent.

An interesting juxtaposition of these positive and negative feedbacks occurs in northern Africa. The sinking motion and dryness over much of the Sahara are intensified through the positive feedback mechanism described above. However, the northern extreme of the Sahara has a response more typical of midlatitudes, with precipitation less responsive to the surface albedo effects, but soil moisture increases because of decreased surface temperature and potential evaporation. These effects together give a southward shift of the Sahara.

The results of the positive feedback at low latitudes are most dramatically displayed in Africa. When land surface albedo is held at a constant value of 0.17, Africa is primarily covered by woods (indicating conditions intermediate between wet and dry). When feedback is allowed, variations in precipitation and soil moisture are magnified, producing very moist tropical rainforests in equatorial Africa and deserts in northern and southwestern Africa, more closely reflecting reality.

As in all GCM studies, the results are dependent on the parameterization schemes used. In particular, the two-step determination of surface albedo based on climate as used here should be viewed with caution, along with the omission of seasonal variability in surface albedo, other than that due to snow. Nevertheless, although quantitative measures of sensitivity and feedback may be dependent on model formulation, it is believed that this exercise using a GCM as a tool has identified physical and biophysical mechanisms by which climatic feedback may be occurring.

Surface albedo is only one surface parameter related to vegetation that may interact with climate and lead to feedback. Lofgren (1993) also investigated the effects of surface roughness and soil water holding capacity. These results are briefly summarized here. It was found that feedback due to soil water holding capacity is always small compared to that due to surface albedo. Feedbacks due to surface roughness are also much smaller than those due to surface albedo at tropical and subtropical latitudes. However, the effect of surface roughness on Ekman convergence means that the high surface roughness of midlatitude forests enhances summer precipitation and soil moisture, giving a positive feedback in areas where surface albedo did not yield a consistent feedback.

Acknowledgments. This paper is taken from material contained in my Ph.D. thesis. It would not have been possible without the firm guidance of Dr. Syukuro Manabe. This work was supported through a NASA Global Change Graduate Student Fellowship. The Geophysical Fluid Dynamics Laboratory provided the necessary computing resources. N.-C. Lau, C. Milly, E. Wood, T. Croley, and P. Dirmeyer are gratefully acknowledged for helpful discussions and comments on early versions of the manuscript, along with two anonymous referees. A. Broccoli, R. Wetherald, and T. Delworth gave assistance in running the GCM. P. Tunison, J. Varanyak, and C. Rafael assisted in preparation of several figures.

REFERENCES

Broccoli, A. J., and S. Manabe, 1992: The effects of orography on midlatitude Northern Hemisphere dry climates. *J. Climate,* **5,** 1181–1201.

Budyko, M. I., 1975: *Climate and Life.* International Geophysics Series, Vol. 18, Academic Press, 508 pp.

Charney, J. G., 1975: Dynamics of deserts and drought in the Sahel. *Quart. J. Roy. Meteor. Soc.,* **101,** 193–202.

Dorman, J. L., and P. J. Sellers, 1989: A global climatology of albedo, roughness length, and stomatal resistance for atmospheric general circulation models as represented by the Simple Biosphere Model (SiB). *J. Appl. Meteor.,* **28,** 833–855.

Gordon, C. T., and W. F. Stern, 1982: A description of the GFDL global spectral model. *Mon. Wea. Rev.,* **110,** 625–644.

Held, I. M., 1985: Stationary and quasi-stationary eddies in the extratropical troposphere: Theory. *Large-Scale Dynamical Processes in the Atmosphere,* B. J. Hoskins and R. P. Pearce, Eds., Academic Press, 127–168.

Henderson-Sellers, A., 1990: Predicting generalized ecosystem groups with the NCAR CCM: First steps towards an interactive biosphere. *J. Climate,* **3,** 917–940.

——, and A. J. Pitman, 1992: Land-surface schemes for future climate models: Specification, aggregation, and heterogeneity. *J. Geophys. Res.,* **97,** 2687–2696.

Holdridge, L. R., 1947: Determination of world plant formations from simple climatic data. *Science,* **105,** 367–368.

Hollander, M., and D. A. Wolfe, 1973: *Nonparametric Statistical Methods.* Wiley, 503 pp.

Köppen, W., 1936: Das geographische System der Klimate. *Handbuch der Klimatologie,* Vol. 1, Part C, W. Köppen and R. Geiger, Eds., Gebruder Borntraeger, 44 pp.

Küchler, A. W., 1982: Natural vegetation. *Goode's World Atlas,* 16th ed., E. B. Espenshade Jr., Ed., Rand McNally and Company, 16–17.

——, 1991: Natural vegetation. *The New International Atlas,* Anniversary ed., Rand McNally and Company, xxxviii–xxxix.

Legates, D. R., and C. J. Willmott, 1990: Mean seasonal and spatial variability in gauge-corrected, global precipitation. *Int. J. Climatol.,* **10,** 111–127.

Li, Z., and L. Garand, 1994: Estimation of surface albedo from space: A parameterization for global application. *J. Geophys. Res.,* **99,** 8335–8350.

Lofgren, B. M., 1993: Sensitivity and feedbacks associated with vegetation-related land surface parameters in a general circulation model. Ph.D. thesis, Princeton University, 206 pp.

——, 1995: Sensitivity of land–ocean circulations, precipitation, and soil moisture to perturbed land surface albedo. *J. Climate,* **8,** 2521–2542.

Oort, A. H., 1983: Global atmospheric circulation statistics, 1958–1973. NOAA Prof. Paper No. 14, 180 pp. + 47 microfiche.

Sellers, P. J., Y. Mintz, Y. C. Sud, and A. Dalcher, 1986: A Simple Biosphere Model (SiB) for use within general circulation models. *J. Atmos. Sci.,* **43,** 505–531.

Sud, Y. C., and W. E. Smith, 1985: Influence of local land-surface processes on the Indian Monsoon: A numerical study. *J. Climate Appl. Meteor.,* **24,** 1015–1036.